ACS APPLIED MATERIALS & INTERFACES

Letter

www.acsami.org

Monolithic Polymer Microlens Arrays with High Numerical Aperture and High Packing Density

Hyukjin Jung and Ki-Hun Jeong*

Department of Bio and Brain Engineering and KAIST Institute for Optical Science and Technology, Korea Advanced Institute of Science and Technology (KAIST), 291 Daehak-ro, Yuseong-gu, Daejeon 305-701, Republic of Korea

S Supporting Information

ABSTRACT: This work reports a novel method for monolithic fabrication of high numerical aperture polymer microlens arrays (high-NA MLAs) with high packing density (PD) at wafer level. The close-packed high-NA MLAs were fabricated by incorporating conformal deposition of ultrathin fluorocarbon nanofilm and melting the cylindrical polymer islands. The NA and PD of hemispherical MLAs with a hexagonal arrangement increase up to 0.6 and 89%, respectively. The increase of NA enhances the lens transmission securing the beam width down to 1.1 μm. The close-packed high-NA MLAs enable high photon collection efficiency with signal-to-noise ratio greater than 50:1.

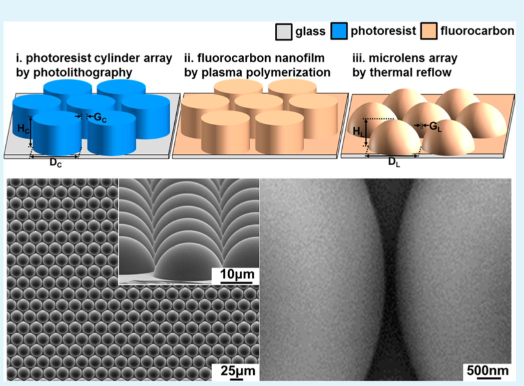

KEYWORDS: *microlens array, ultrathin fluorocarbon, hydrophobic effect, surface energy, thermal reflow*

Polymer microlens arrays (MLAs) are being widely utilized for optical sensors,[1−3] 3D displays,[4,5] lighting devices,[6−9] 4D light-feld cameras; microscopes,[10−12] and photovoltaic cells,[13,14] as well as in optofluidic lab-on-a chip devices.[15,16] From a practical standpoint, increasing both numerical aperture (NA) and packing density (PD) of MLAs spurs remarkable augmentation of light collection or extraction efficiency.[9,10,13] Consequently, the batch fabrication of such MLAs drives the integrated optical systems in high photosensitivity at low cost. For instance, monolithic polymer MLAs with high NA provide substantial benefits for improving photon collection onto the image sensor arrays (ISA) of charge-coupled device (CCD) or complementary metal−oxide−semiconductor (CMOS). Furthermore, polymer MLAs with high packing density ensure high signal-to-noise ratio detection while increasing the pixel density of ISA. Among many different methods for monolithic integration of refractive polymer MLAs, a resist melting method, i.e., thermal reflow of cylindrical polymer micropatterns over the glass transition temperature (T_g) to form the lenslets by the surface energy minimization,[17] has been widely used in industrial applications owing to the facility of direct integration, large area fabrication, and precise alignment with ISA.[18,19] In practice, however, technical realization of high-NA MLAs simultaneously without sacrificing the packing density is still challenging in using conventional resist melting methods. The lenslet profile substantially depends on the surface energy of a substrate, whose high surface energy hampers the monolithic fabrication of close-packed high-NA MLAs due to the union between adjacent micropatterns during the resist melting.[20] As a result, conventional resist melting is still challenging in forming close-packed high-NA MLAs. Although previous methods using the hydrophobic effect[29−31] can offer the direct fabrication of high-NA MLAs on the hydrophilic domains with multiple dipping of the patterned chip into the monomer solution, NA is still limited below 0.42. In addition, the technical difficulty in the precise control of monomer volume hampers high-PD MLAs because of the coalescence of liquid droplets in that the minimum gap between microlenses is limited by the standard photolithographic resolution (λ = 365 nm). The fabrication of close-packed high-NA polymer MLAs have been more recently demonstrated by employing soft-lithographic replication of MLA templates resulting from two-step UV lithography,[21] microsphere lithography,[22] and laser ablation-assisted wet etching[23] or direct laser writing.[24] However, all the previous methods still have technical difficulties in simple control of lens profiles, low-cost large-area fabrication, and precise alignment with ISA at wafer level.

This work reports the simple and monolithic fabrication of close-packed high-NA polymer MLAs at wafer level. The batch nanofabrication was done by melting cylindrical polymer micropatterns covered with plasma-induced fluorocarbon nanofilm (FC nanofilm) as illustrated in Figure 1a. A positive tone photoresist (AZ 9260, AZ Electronic Materials) was initially defined as cylindrical micropatterns on a 4-in borofloat glass wafer by using conventional photolithography. The FC nanofilm was conformally deposited on both the surfaces of micropatterns and glass substrate in ambient condition by incorporating

Received: November 7, 2014
Accepted: January 23, 2015
Published: January 23, 2015

DOI: 10.1021/am5077809
ACS Appl. Mater. Interfaces 2015, 7, 2160−2165

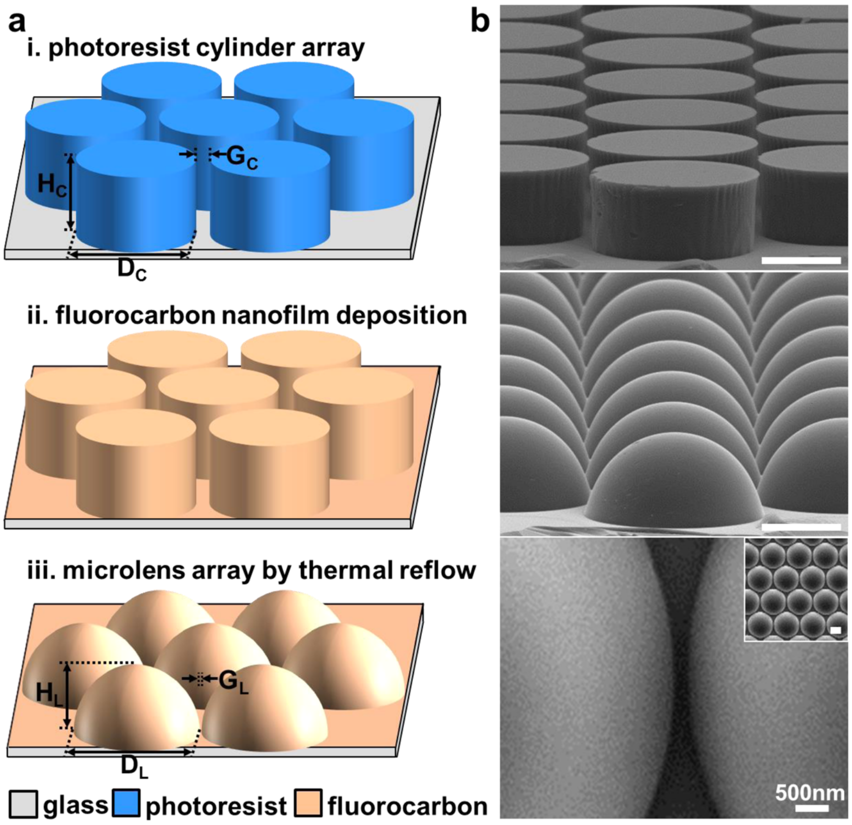

Figure 1. Monolithic polymer microlens arrays (MLAs) with high numerical aperture (NA) and high packing density (PD). (a) Nano- and microfabrication procedures of close-packed high-NA polymer MLAs by incorporating conformal deposition of fluorocarbon nanofilm and thermal reflow. The lens profiles (diameter: D_L and height: H_L) and packing density of MLAs can be precisely controlled by the geometrical parameters of cylindrical micropatterns (diameter: D_C and height: H_C) of close packing. (b) SEM images of close-packed high-NA MLAs (middle) with the interstitial gap spacing of ~200 nm between microlenses (bottom) after thermal annealing of close-packed polymer micropatterns with high aspect ratio (top). Scale bar: 10 μm (top, middle, and inset panel).

plasma-induced polymerization of perfluorocyclobutane (C_4F_8) precursor under radiofrequency (RF) power of 150 W, helium gas of 5 L/min, and C_4F_8 gas of 2 sccm (IHP-1000, APP Korea). Finally, the cylindrical polymer micropatterns were melted and hardened by thermal cross-linking at 180 °C for 30 min in a convection oven. Note that the lens profile (diameter: D_L and height: H_L) and the packing density (PD) of MLAs are determined by the geometrical parameters of cylindrical micropattern (diameter: D_c and height: H_c). The SEM images clearly demonstrate close-packed high-NA MLAs successfully fabricated from close-packed cylindrical micropatterns with high aspect ratio without the union securing the nanogap between polymer microlenses unlike conventional resist reflow methods (Figure 1b).

The FC nanofilm plays a crucial role in the uniform formation of close-packed spherical MLAs during thermal reflow.[28] The surface contact angle of deionized water on a glass substrate increases from 15 to 110° as the FC nanofilm increases from 0 to 4 nm in thickness, which was measured by using a spectroscopic ellipsometer (M2000D, Woollam). Moreover, the FC nanofilm provides the substrate independent hydrophobicity. In particular, the FC nanofilm over 4 nm in thickness effectively provides hydrophobic effect on the substrate without regressing to the hydrophilic state due to high temporal stability (see Figure S1 in the Supporting Information). The SEM images show the normal lens surfaces (top), the planarized surface after the lens union (middle), and the high-NA lens surfaces (bottom) after melting the polymer cylinders with and without the presence of FC nanofilm, respectively (Figure 2). The lens profiles extracted from the cross-sectional SEM images by using ImageJ software clearly demonstrate that the initial FC thickness of 4 nm effectively secures the spherical profile of MLAs after thermal annealing without the union between densely packed cylindrical micropatterns with a gap spacing (i.e., G_C/D_C) of 0.24 (Figure 2). Conventional polymer micropatterns are transformed into normal microlenses with 0.12 of the aspect ratio (AR), i.e., H_C/D_C, however, they become directly merged due to the rapid increase of the initial D_C as the AR slightly increases up to 0.21. High surface energy of the substrates causes rapid spreading of D_L with the small increase in AR, thereby hindering both the precise control of lens profile and the increase of PD. In contrast, this hydrophobic FC nanofilm offers the uniform formation of high-NA MLAs without sacrificing the PD for cylindrical micropatterms with high AR over 0.63 while securing excellent surface quality with surface roughness of 2 ± 0.1 nm (see Figure S2 in the Supporting Information). Consequently, the FC nanofilm-assisted thermal reflow (FC-reflow) further delivers great advantages for high-NA and high-PD MLAs unlike conventional methods.

The lens size, i.e., the diameter D_L and the height H_L, of a spherical microlens can be simply determined by the initial AR of a cylinder micropattern according to the contact angle between a microlens and a substrate (Figure 3a and Figure S3 in the Supporting Information). The experimental results show the relationship between the AR and the γ/η, where γ and η

DOI: 10.1021/am5077809
ACS Appl. Mater. Interfaces 2015, 7, 2160−2165

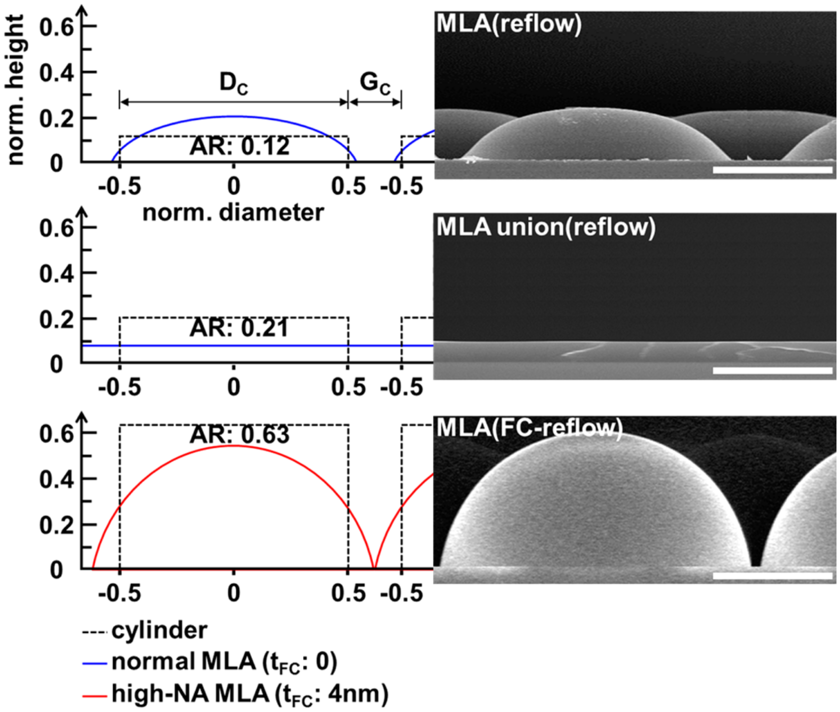

Figure 2. Fluorocarbon nanofilm coated high-NA polymer MLAs without the union between cylindrical polymer micropatterns during thermal reflow: Different lens profiles on the glass substrate after thermal reflow depending on the aspect ratio of polymer cylinders in close packing with the G_C/D_C of 0.24 (left panel). The cross-sectional SEM images of normal lens surfaces (top), planarized surface (middle), and hemispherical lens surfaces (bottom) with and without the presence of 4 nm thick FC nanofilm (right panel). Scale bar: 10 μm.

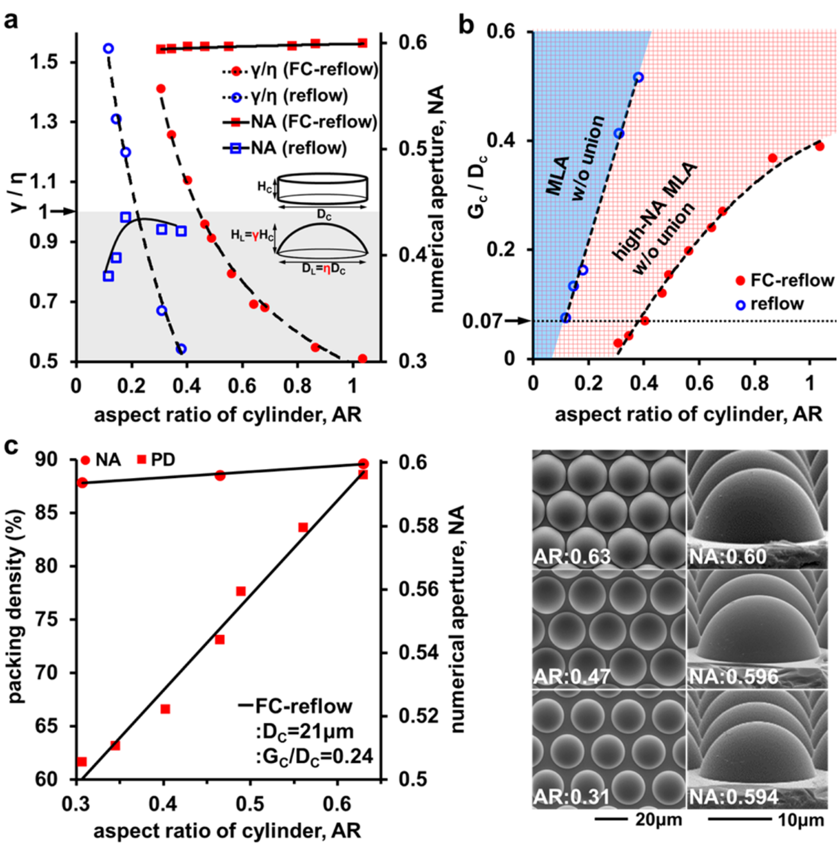

Figure 3. Numerical aperture (NA) and packing density (PD) of polymer MLAs. (a) NAs and γ/η, i.e., $\gamma = H_L/H_C$ and $\eta = D_L/D_C$, of conventional and FC-reflow enabled MLAs depending on the aspect ratio (AR) of initial cylindrical micropatterns. (b) The design rule for controlling the interstitial gap spacing between microcylinders (G_C/D_C) depending on the AR for closely packing of high-NA MLAs (depicted as check boxes in red) and normal MLAs (depicted as blue) without the union between microlenses, where the blank circles and filled circles indicate the minimum G_C/D_C for zero of D_L. (c) NA and PD of polymer MLAs by using FC-reflow depending on the aspect ratio (AR) from G_C/D_C of 0.24. SEM images of polymer MLAs with 0.594, 0.596, and 0.6 of NA resulting from 0.31, 0.47, 0.63 in AR for the initial cylindrical patterns, respectively.

DOI: 10.1021/am5077809
ACS Appl. Mater. Interfaces 2015, 7, 2160−2165

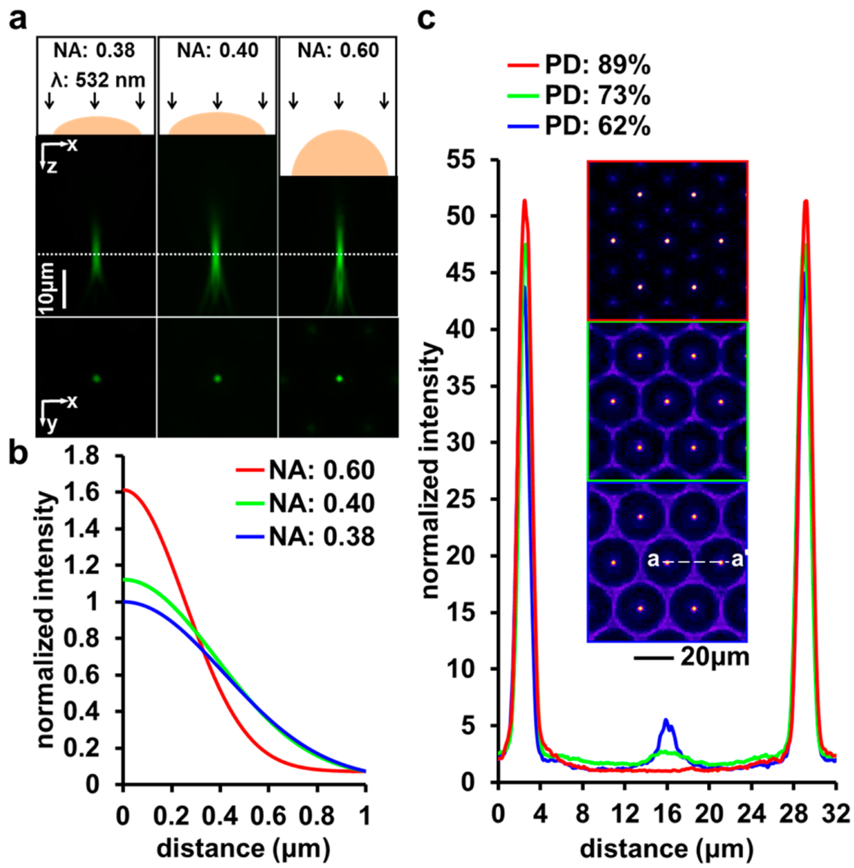

Figure 4. Photon collection enhancement of close-packed high-NA MLAs. (a, b) 3D optical sectioning of coupled light (λ: 532 nm) and PSFs through conventional and hemispherical MLAs depending on NA. (c) Intensity profiles along the line between the foci of high-NA MLAs depending on PD.

correspond to a ratio of H_L/H_C and D_L/D_C, respectively. For a constant diameter of a microlens, the thicker the H_C the higher the H_L, which results in increasing the NA of a spherical microlens as long as H_L is smaller than half the D_L. For instance, a spherical microlens has the maximum NA at $D_L = 2H_L$ as shown in the below

$$\begin{aligned} \mathrm{NA} &= (n-1)\frac{D_L}{2R_C} \\ &= (n-1)\frac{4H_L D_L}{4{H_L}^2 + {D_L}^2} \\ &= (n-1)\frac{4\left(\frac{\gamma}{\eta}\right)(\mathrm{AR})}{4\left(\frac{\gamma}{\eta}\right)^2(\mathrm{AR})^2 + 1} \end{aligned} \quad (1)$$

where R_C is the radius of curvature, n is the refractive index of lens polymer, and AR is the aspect ratio of the cylinder micropattern, i.e., H_C/D_C. However, a small contact angle between the polymer melt and the conventional substrate during thermal reflow still hampers the increase in NA because the increase in η is relatively higher than the reduction in γ for high AR. For example, the NA slightly increases from 0.38 to 0.43 as the AR increases from 0.11 to 0.18, of which the increase is limited by the contact angle of lens polymer in a viscous flow state on the glass substrate. In contrast, the experimental results successfully demonstrate that thermally stable FC nanofilm substantially reduces the increase of η due to the decrease of the substrate surface energy and therefore substantially increases the NA up to the theoretical maximum of 0.6 (from the refractive index of lens polymer, n, 1.6).[25] In addition, a ratio of the initial gap spacing (G_C) between cylindrical micropatterns to the D_C, i.e., G_C/D_C, is also a crucial factor for increasing the PD of MLAs during thermal reflow. Figure 3b presents a design rule for the monolithic fabrication of close-packed high-NA MLAs as a function of AR. The blank circles and filled circles were plotted by $1 - \eta$ according to $G_C + D_C = G_L + \eta D_C$, assuming the G_L is 0 for the normal reflow and the FC-reflow, respectively. For example, closely packed high-NA MLAs with G_C/D_C of 0.07 can be achieved from the cylindrical micropatterns of 0.3 to 0.4 in AR (area depicted as check boxes in red). However, the conventional reflow method significantly hinders the increase of both NA and PD due to the difficulty in the precise control of small AR below 0.1 (area depicted as blue), resulting in the lens union for over the AR of 0.1. Consequently, this experimental result clearly indicates that the pixel density of ISA can be further increased by virtue of the closely packed high-NA MLAs with the minimum initial G_C. Herein, the critical dimension (CD) of the G_C can be decreased by using advanced photolithography such as deep-ultraviolet (DUV) lithography. Furthermore, the increase of AR simply enables the monolithic fabrication of polymer MLAs both high NA and high PD. The experimental results demonstrate the PD of MLAs with a hexagonal arrangement linearly increases from 62 to 89% as the AR increases from 0.31 to 0.63. It is because the D_L spreads from 21.4 to 25.8 μm while the lens gap (G_L) significantly reduces from 4.6 to 0.2 μm (Figure 3c and Figure 1b). The lens pitch (P_X)

DOI: 10.1021/am5077809
ACS Appl. Mater. Interfaces 2015, 7, 2160−2165

remains constant to 26 μm. Note that the hexagonal arrangement of circular microlenses provides the maximum packing density of 90.7%, assuming no gap between the lenses.[26] The experimental results also demonstrate that the NA increases up to 0.6 from the AR of 0.63.

The optical performance of close-packed high-NA MLAs was measured depending on NA and PD. First, the lens transmissions of hemispherical MLAs and normal MLAs were characterized with a modified confocal laser scanning microscope (CLSM) by sequentially imaging the optical sections along the focusing beam under a collimated laser beam at 532 nm.[27] The CLSM (LSM510, Carl Zeiss GmbH) images in x–y plane indicate the excellent spatial uniformity of beam spots at foci of spherical high-NA MLAs. The optical sections in x–z plane also show the focal length (f) of MLAs decreases as the NA increases (Figure 4a). The measured focal lengths were 32, 32, and 21 μm for MLAs depending on the NA of 0.38, 0.40, and 0.60, respectively. The experimental results well match with the calculated focal lengths of 31.3, 31.4, and 20.9 μm based on $f = D_L/2NA$. The point spread function (PSF) was then extracted from the beam spots of individual microlenses. The PSFs clearly demonstrate the light intensity increases by 60% as the NA increases from 0.38 to 0.6 whereas high-NA MLAs (NA: 0.6) secure the beam spot diameter down to 1.1 μm (full width at $1/e^2$ maximum), which is the smallest size ever reported. Figure 4b also clearly demonstrates that further dense packing of high-NA MLAs enables high signal-to-noise ratio (SNR) detection over 50:1 by maximizing the photon collection efficiency, i.e., the enhancement of light transmission through high-NA microlens and the sharp cutoff of noise passing through the microlens intervals at a subwavelength scale.

In summary, this work successfully demonstrates a simple and effective method for monolithic polymer microlens arrays with both high NA and high PD at wafer level by melting the cylindrical polymer micropatterns after the conformal deposition of plasma-induced FC nanofilm. The lens shape can be precisely controlled by the FC nanofilms serving as a hydrophobic layer. Furthermore, the lens size and the PD for close-packed high-NA MLAs were simply determined by the single control variable of AR. The close-packed high-NA MLAs exhibit high PD and NA up to 89% and 0.6, respectively. The results clearly demonstrate that further close packing of high-NA MLAs increase the SNR of 50:1 due to the significant enhancement of photon collection efficiency. To the best of our knowledge, this MLA offers the highest figures of merits among the close-packed high-NA MLAs ever reported up to now, considering NA, beam diameter, PD, and large-area fabrication cost at wafer level. This simple method can provide great potentials for diverse optical applications such as high resolution imaging and projection lithography systems, solid immersion lenses (SIL), and more. Besides, close-packed hemispherical MLAs and their replicas can be further extended toward fully integrated micro total analysis systems (μTAS) for high-throughput screening and highly sensitive detection.

■ ASSOCIATED CONTENT

Ⓢ Supporting Information

The experimental results support ultrathin fluorocarbon nanofilms (FC nanofilms) provide hydrophobicity regardless of what substrates are used (Figure S1). The experimental results support FC nanofilms secure smooth surfaces of microlens arrays (Figure S2). The numerical and experimental results support the quantitative estimation of lens profiles by using an analytical model for resist melting (Figure S3). This material is available free of charge via the Internet at http://pubs.acs.org/.

■ AUTHOR INFORMATION

Corresponding Author

*E-mail: kjeong@kaist.ac.kr. Phone: +82.42.350.4323. Fax: +82.42.350.4310.

Notes

The authors declare no competing financial interest.

■ ACKNOWLEDGMENTS

This work is supported by the National Research Foundation of Korea (NRF) grant funded by the Korea government (MEST) (2014022751, 2014039957, 2011-0031866, 10041120).

■ REFERENCES

(1) Jung, H.; Jeong, K.-H. Monolithic Polymer Microlens Arrays with Antireflective Nanostructures. *Appl. Phys. Lett.* **2012**, *101*, 203102.

(2) Kang, D.; Pang, C.; Kim, S. M.; Cho, H. S.; Um, H. S.; Choi, Y. W.; Suh, K. Y. Shape-Controllable Microlens Arrays via Direct Transfer of Photocurable Polymer Droplets. *Adv. Mater.* **2012**, *24*, 1709–1715.

(3) Stoklasa, B.; Motka, L.; Rehacek, J.; Hradil, Z.; Sánchez-Soto, L. L. Wavefront Sensing Reveals Optical Coherence. *Nat. Commun.* **2014**, *5*, 3275.

(4) Lanman, D.; Luebke, D. Near-Eye Light Field Displays. *ACM Trans. Graph.* **2013**, *32*, 1–10.

(5) Xiao, X.; Javidi, B.; Martinez-Corral, M.; Stern, A. Advances in Three-Dimensional Integral Imaging: Sensing, Display, and Applications [Invited]. *Appl. Opt.* **2013**, *52*, 546–560.

(6) Sun, Y.; Forrest, S. R. Enhanced Light Out-Coupling of Organic Light-Emitting Devices Using Embedded Low-Index Grids. *Nat. Photonics* **2008**, *2*, 483–487.

(7) Yang, J. P.; Bao, Q. Y.; Xu, Z. Q.; Li, Y. Q.; Tang, J. X.; Shen, S. Light Out-coupling Enhancement of Organic Light-emitting Devices with Microlens Array. *Appl. Phys. Lett.* **2010**, *97*, 223303.

(8) Thomschke, M.; Reineke, S.; Lüssem, B.; Leo, K. Highly Efficient White Top-Emitting Organic Light-Emitting Diodes Comprising Laminated Microlens Films. *Nano Lett.* **2011**, *12*, 424–428.

(9) Wrzesniewski, E.; Eom, S.-H.; Cao, W.; Hammond, W. T.; Lee, S.; Douglas, E. P.; Xue, J. Enhancing Light Extraction in Top-Emitting Organic Light-Emitting Devices Using Molded Transparent Polymer Microlens Arrays. *Small* **2012**, *8*, 2647–2651.

(10) Ng, R.; Levoy, M.; Brédif, M.; Duval, G.; Horowitz, M.; Hanrahan, P. Light Field Photography with A Hand-Held Plenoptic Camera. *Computer Science Technical Report CSTR* **2005**, *2*, 1–11.

(11) Orth, A.; Crozier, K. Microscopy with Microlens Arrays: High Throughput, High Resolution and Light-Field Imaging. *Opt. Express* **2012**, *20*, 13522–13531.

(12) Kim, J.; Jung, J.-H.; Jeong, Y.; Hong, K.; Lee, B. Real-Time Integral Imaging System for Light Field Microscopy. *Opt. Express* **2014**, *22*, 10210–10220.

(13) Myers, J. D.; Cao, W.; Cassidy, V.; Eom, S.-H.; Zhou, R.; Yang, L.; You, W.; Xue, J. A Universal Optical Approach to Enhancing Efficiency of Organic-Based Photovoltaic Devices. *Energy Environ. Sci.* **2012**, *5*, 6900–6904.

(14) Chen, Y.; Elshobaki, M.; Ye, Z.; Park, J.-M.; Noack, M. A.; Ho, K.-M.; Chaudhary, S. Microlens Array Induced Light Absorption Enhancement in Polymer Solar Cells. *Phys. Chem. Chem. Phys.* **2013**, *15*, 4297–4302.

(15) Lim, J.; Gruner, P.; Konrad, M.; Baret, J.-C. Micro-Optical Lens Array for Fluorescence Detection in Droplet-Based Microfluidics. *Lab Chip* **2013**, *13*, 1472–1475.

(16) Lim, J.; Vrignon, J.; Gruner, P.; Karamitros, C. S.; Konrad, M.; Baret, J.-C. Ultra-High Throughput Detection of Single Cell β-galactosidase Activity in Droplets Using Micro-Optical Lens Array. *Appl. Phys. Lett.* **2013**, *103*, 203704.

DOI: 10.1021/am5077809
ACS Appl. Mater. Interfaces 2015, 7, 2160–2165

(17) O'Neill, F. T.; Sheridan, J. T. Photoresist Reflow Method of Microlens Production Part I: Background and Experiments. *Optik−Int. J. Light Electron Optics* **2002**, *113*, 391−404.
(18) Popovic, Z. D.; Sprague, R. A.; Connell, G. A. N. Technique for Monolithic Fabrication of Microlens Arrays. *Appl. Opt.* **1988**, *27*, 1281−1284.
(19) Volkel, R.; Eisner, M.; Weible, K. J. Miniaturized Imaging Systems. *Microelectron. Eng.* **2003**, *67*−*68*, 461−472.
(20) Roy, E.; Voisin, B.; Gravel, J. F.; Peytavi, R.; Boudreau, D.; Veres, T. Microlens Array Fabrication by Enhanced Thermal Reflow Process: Towards Efficient Collection of Fluorescence Light From Microarrays. *Microelectron. Eng.* **2009**, *86*, 2255−2261.
(21) Hsin-Ta, H.; Guo-Dung John, S. A Novel Boundary-Confined Method for High Numerical Aperture Microlens Array Fabrication. *J. Micromech. Microeng.* **2010**, *20*, 035023.
(22) Eom, S.-H.; Wrzesniewski, E.; Xue, J. Close-Packed Hemispherical Microlens Arrays for Light Extraction Enhancement in Organic Light-Emitting Devices. *Org. Electron.* **2011**, *12*, 472−476.
(23) Xiangwei, M.; Feng, C.; Qing, Y.; Hao, B.; Hewei, L.; Pubo, Q.; Yang, H.; Jinhai, S.; Xun, H. A Simple Way to Fabricate Close-Packed High Numerical Aperture Microlens Arrays. *IEEE Photonics Technol. Lett.* **2013**, *25*, 1336−1339.
(24) Wu, D.; Wu, S.-Z.; Niu, L.-G.; Chen, Q.-D.; Wang, R.; Song, J.-F.; Fang, H.-H.; Sun, H.-B. High Numerical Aperture Microlens Arrays of Close Packing. *Appl. Phys. Lett.* **2010**, *97*, 031109.
(25) Park, J.; Wang, S.; Li, M.; Ahn, C.; Hyun, J. K.; Kim, D. S.; Kim, D. K.; Rogers, J. A.; Huang, Y.; Jeon, S. Three-Dimensional Nanonetworks for Giant Stretchability in Dielectrics and Conductors. *Nat. Commun.* **2012**, *3*, 916.
(26) Nussbaum, P.; Volke, R.; Herzig, H. P.; Eisner, M.; Haselbeck, S. Design, Fabrication and Testing of Microlens Arrays for Sensors and Microsystems. *Pure Appl. Opt.* **1997**, *6*, 617−636.
(27) Jeong, K.-H.; Kim, J.; Lee, L. P. Biologically Inspired Artificial Compound Eyes. *Science* **2006**, *312*, 557−561.
(28) Yan Xin, Z.; Aric, M. Wettability and Thermal Stability of Fluorocarbon Films Deposited by Deep Reactive Ion Etching. *J. Vac. Sci. Technol., A* **2005**, *23*, 434−439.
(29) Biebuyck, H. A.; Whitesides, G. M. Self-Organization of Organic Liquids on Patterned Self-Assembled Monolayers of Alkanethiolates on Gold. *Langmuir* **1994**, *10*, 2790−2793.
(30) Hartmann, D. M.; Kibar, O.; Esener, S. C. Characterization of a Polymer Microlens Fabricated by Use of the Hydrophobic Effect. *Opt. Lett.* **2000**, *25*, 975−977.
(31) Wei, H. C.; Su, G. D. J. Using Hydrophilic Effect to Fabricate Self-Assembled Microlens Array by UV/Ozone Modification. *IEEE Photonics Technol. Lett.* **2012**, *24*, 300−302.

DOI: 10.1021/am5077809
ACS Appl. Mater. Interfaces 2015, 7, 2160−2165